Hexagonal Ce1-xLnx(OH)CO3 as highly efficient precursors of nanocrystalline Ln(III-IV)-substituted ceria.

Journal:	*Crystal Growth & Design*
Manuscript ID	Draft
Manuscript Type:	Article
Date Submitted by the Author:	n/a
Complete List of Authors:	Sorbello, Cecilia; Facultad de Ciencias Exactas y Naturales, Universidad de Buenos Aires, DQIAQF Jobbagy, Matias; Universidad de Buenos Aires, Inorganic Chemistry

Hexagonal $Ce_{1-x}Ln_x(OH)CO_3$ as highly efficient precursors of nanocrystalline Ln(III-IV)-substituted ceria.

Cecilia Sorbello[a] and Matias Jobbágy[a]*

a INQUIMAE, DQIAQF, Facultad de Ciencias Exactas y Naturales, Universidad de Buenos Aires, Pabellón II, Ciudad Universitaria, C1428EHA-Buenos Aires, Argentina.

Corresponding author: jobbag@qi.fcen.uba.ar

Abstract

Monophasic hexagonal precursors, obeying to the formula $Ce_{1-x}Ln_x(OH)CO_3$, are introduced herein as versatile precursors for the obtainment of Ln(III-IV) substituted nanocrystalline ceria. To this aim, three hexagonal $Ce_{1-x}Ln_x(OH)CO_3$ families increasingly substituted with Ln(III)=Sm(III), Gd(III) or Pr(III), were prepared with high (quantitative) precipitation yields. Once $Ce_{1-x}Ln_x(OH)CO_3$ precursors are submitted to moderate thermal treatment (5 h, 723 K, air atmosphere), the oxidation of Ce(III) centers triggers a single step massive decomposition (dehydroxilation/decarbonatation), developing monophasic $Ce_{1-x}Ln_xO_{2-\delta}$ solid solutions with Ln(IV-III) substitutions up to 30%. These binary oxides exhibit large surface areas, up to 130 m^2 g^{-1}, even larger than those obtained by means of costly procedures.

1. Introduction

Ceria and related lanthanide (Ln) substituted CeO_2-like phases play a key role in current development of clean energy technologies. The unique redox chemistry of the reversible Ce(III)/Ce(IV) redox pair results in stable oxides holding a high oxygen storage capacity (OSC)[1,2] and eventually, ionic conductivity.[3] On one hand, these phases textured in the form of high surface area nanoparticles or mesoporous monolithic catalysts, are able to minimize the impact of established technologies as combustion motors, providing effective exhaust treatment including CO oxidation,[4,5] combustion of organic compounds[6] or three way catalysts.[7] On the other, their high ionic conductivity reached at moderate temperatures (above 600 ^oC), allows their application as electrolytes for intermediate temperature solid oxide fuel cells.[8,9] In both scenarios, the obtainment of phases exhibiting optimum Ln(III-IV)-Ce(IV) interdispersion (solid solution) combined with textural control is mandatory.[10]

Several preparative strategies can be found in literature, ranging from sophisticated procedures based on molecular templates or micro emulsions, involving non-green and costly solvents and/or surfactants.[11,12] In the search of high yield sustainable procedures, thermal decomposition of suitable crystalline precursors prepared by the urea method arise as green water based alternative that prevents the use of aggressive starting reagents or the release of harmful byproducts.[13] Carboxylates,[14] carbonates,[15] basic carbonates,[16] basic chlorides,[17] layered double salts[18,19] or layered double hydroxides[20] revealed an enormous potential as precursors for nanocrystalline multicationic oxides, either as stable solid solutions[21] or metastable phases of tuned stoichiometry.[22] In particular, the thermal treatment of crystalline $Ce_{1-x}La_x(OH)CO_3$ demonstrated to allow the high yield obtainment of nanocrystalline $Ce_{1-x}La_xO_{2-\delta}$ oxides under mild temperatures.[23,24] Based on this strategy, the present paper explores the thermal decomposition of several $Ce_{1-x}Ln_x(OH)CO_3$ phases as precursors of nanotextured $Ce_{1-x}Ln_xO_{2-\delta}$. In order to evaluate the role the inherent redox stability of employed Ln(III), either stable Sm(III) or Gd(III) as well as non-stable Pr(III) were evaluated. Finally, the catalytic activity of nanotextured $Ce_{1-x}Ln_xO_{2-\delta}$ towards CO oxidation as a function of Ln content is also analyzed.

2. Experimental

2.1. Synthesis and chemical characterization of precursors. Precursors were prepared by the urea method,[13] by aging several solutions containing Cerium(III) nitrate and Ln(III) nitrate (keeping a total cationic concentration of 0.1 mol dm^{-3}) with urea (0.5 mol dm^{-3}). Typically 50 cm^3 of each solution was filtered, bubbled with nitrogen and aged at 473.0 ± 0.5 K for 10 days in Teflon lined autoclaves. The precipitated solids were collected by filtration through 0.2 μm pore size cellulose nitrate membranes, washed three times with cold water, and dried at 373 K overnight. Ln(III) to Ce(III) ratio in the solid was assessed by ICP analyses. Remnant Ln(III) and Ce(III) in mother liquor indicate a precipitation yield higher than 99.5 ± 0.5 %. Carbon elemental analyses were carried out in a Carlo Erba CHON-S analyzer.

2.2. Thermal treatment of precursors. Precursors thermal stability was explored by TGA (Shimadzu TG 51) analysis, heating the samples under air flow (50 cm^3 min^{-1}) at 1.0 K min^{-1} from room temperature to 1173 K, and holding the final temperature for 30 min. Mixed oxides were obtained by heating precursors under an air flow (50 cm^3 min^{-1}) at 5.0 K min^{-1} from room temperature to 723 K and holding these value for 5 h.

2.3. Characterization of solids. All synthesized solids were characterized by powder X-ray diffraction (PXRD) using a graphite-filtered Cu K_α radiation (λ=1.5406 Å), scanning electron microscopy (SEM), energy dispersive X-ray spectroscopy (EDS) and Fourier-transform infrared spectroscopy (FTIR). Nitrogen sorption isotherms were performed at 77 K on an ASAP 2020 apparatus; surface area was estimated based on Langmuir's model.

3. Results and discussion

3.1. Synthesis, chemical characterization and yield of precursors

All the samples were prepare from parent nitrates salts except Pr(III)-Ce(III) samples, that developed partial oxidation on certain binary samples. The formation of these undesired impurities was avoided employing chloride salts instead. The ratio [urea] / ($[Ce(III)]_o$ + $[Ln(III)]_o$) was kept constant at 5 in all preparations and the Ln(III) cationic percentage, 100 [Ln(III)] / ([Ln(III)] + [Ce(III)]), was explored in the range 0-50. Samples were labeled as LnX where X represents the cationic percentage; bare Ln100 were prepared as reference for thermal decomposition exploration. Due to the excess of urea employed, the precipitation of all samples reached a final pH value of 9.20, imposed by the NH_4^+/NH_3 buffer. Under such conditions the precipitation of both Ce(III) and Ln(III) cations was quantitative, resulting in a yield of 22 g of $Ce_{1-x}Ln_x(OH)CO_3$ per dm^3.

3.2. Structure of Ln(III)-Ce(III) precursors

Figure 1 shows the PXRD patterns recorded for Ce(III)-Pr(III) set of samples; all samples can be indexed as hexagonal (*P62c* symmetry) Ce(III) basic carbonate ($Ce(OH)CO_3$; PDF 52-0352). The strong signal of the most stable form of Ln(III) basic carbonates in addition with the absence of the kinetically preferred orthorhombic phase confirmed the effectiveness of aging.[25,26]

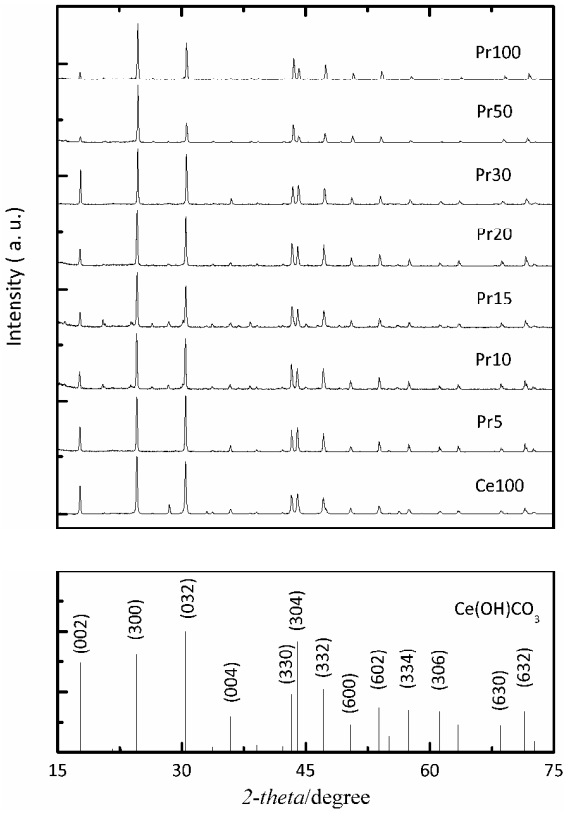

Figure 1 Upper panel: PXRD patterns of binary precursors Ce(III)-Pr(III) with increasing Pr(III) content. Lower panel: main reflections of hexagonal $Ce(OH)CO_3$ reference (PDF 52-0352).

Similar results were observed for Ce(III)-Sm(III) set, were hexagonal phase is observed up to a 50% of Sm(III) substitution (see Figure 2). However bare Sm(III) crystallized in the form of orthorhombic $Sm(OH)CO_3$ (PDF 41-0663).[27] The Ce(III)-Gd(III) set also presents the hexagonal structure up to 30% of substitution while for compositions ranging from 50 to 100%, bare carbonate $Gd_{2-x}Ce_x(CO_3)_3$ (PDF 37-0559) was the only crystalline phase observed, in agreement with previous reports (see Figure S1).[28] Once confirmed the occurrence of monophasic products, the dependence of cell parameters as a function of Ln(III) substitution was explored. Figure 3 compiles the dependence of cell volume for all the hexagonal Ce(III)-Ln(III) compounds obtained herein as well as $Pr(OH)CO_3$, $Sm(OH)CO_3$ and $Gd(OH)CO_3$ reference hexagonal phases. For the three hexagonal set of binary compounds families, a continuous contraction with increasing Ln(III) contents can be observed. For each set, these values agree with the linear trend predicted by Vegard´s law for solid solutions, indicating the occurrence of a binary monophasic $Ce_{1-x}Ln_x(OH)CO_3$ within the aforementioned ranges.[29]

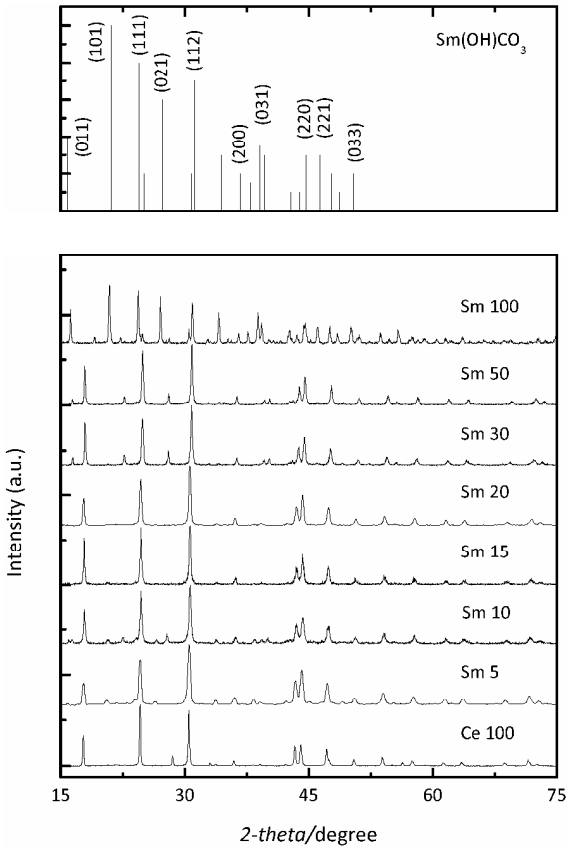

Figure 2 Lower panel: PXRD patterns of binary precursors Ce(III)-Sm(III) with increasing Sm(III) content. Upper panel: main reflections of orthorhombic $Sm(OH)CO_3$ reference (PDF 41-0663).

The occurrence of solid solution with La(III)[24] and Pr(III) in the whole range of compositions is not surprising; it was observed in related systems that Ce(III) tend to share the same lattice with La(III) and Pr(III) due to their similar radii and coordination environments.[30] However, Gd(III) and Sm(III) tend to adopt lower coordination environments due to lanthanide contraction.[31]

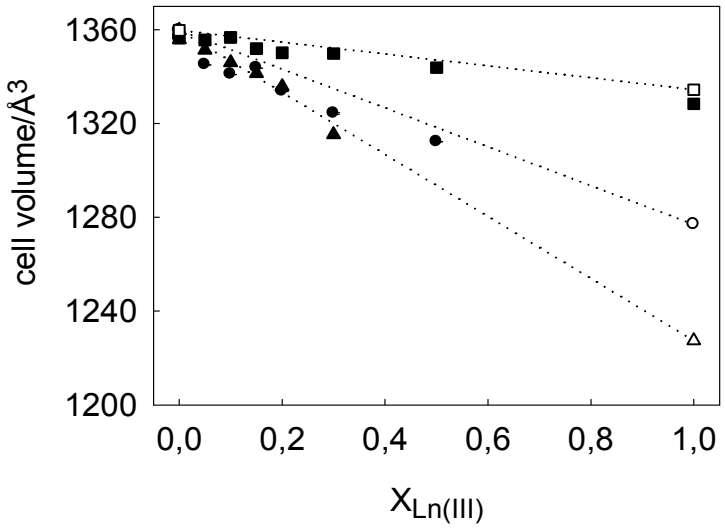

Figure 3. Cell volume of $Ce_{1-x}Ln_x(OH)CO_3$ precursors as a function of Ln(III) content, $X_{Ln(III)}$, with Ln(III) = Sm(III) (filled circles), Gd(III) (filled triangles) and Pr(III) (filled squares). Reference values (empty symbols) of hexagonal $Sm(OH)CO_3$ (PDF 26-0948), $Gd(OH)CO_3$ (PDF 24-0421), Pr(OH)CO3 (PDF 27-1376) and $Ce(OH)CO_3$ (PDF 52-0352) were also added for comparison.

The hexagonal samples present the characteristic FTIR spectra recorded for hexagonal $Ce_{1-x}La_x(OH)CO_3$ (see Figure S2).[24,32] Hydroxyl groups present three ν bands (centered at 3631, 3487 and 3618 cm^{-1}) and one band corresponding to a δ mode (at 595 cm^{-1}). Two triplets (1512, 1435, 1408 and 872, 849 and 777 cm^{-1}) corresponding to the ν_3 and the ν_2 modes of ion $CO_3^{=}$ and a duplet (727 and 706 cm^{-1}) corresponding to the ν_4 vibration confirm the presence of non-equivalents groups within the structure. The complexity of the spectra agrees with the presence of six $CO_3^{=}$, three Ln(III), and five non-equivalent OH^- groups that characterize the hydroxyl-bastnaesite structure.[33] The chemical analysis of the obtained samples confirmed the phases indicated by PXRD analysis; FESEM inspection revealed well developed polycrystalline particles of 1 μm. The absence of the typical spherical particles of quasi-amorphous $Ln(OH)CO_3.H_2O$ or the ellipsoids of orthorhombic $Ln(OH)CO_3$ confirmed the effectiveness of total recrystallization process (data not shown).[31,33–37]

3.3. Thermal decomposition of Ln(III)-Ce(III) precursors

Preliminary reports revealed that under an oxygen atmosphere, either orthorhombic or hexagonal $Ce(OH)CO_3$ decompose in a single step centered at 550 K. Simultaneous decarbonation and dehydroxilation is triggered by Ce(III) oxidation (eq. 1, Table 1).[38,39] Further annealing oxidizes remnant Ce(III)-rich shell belonging to a nanometric $CeO_{2-\delta}$ phase.[40,41] This behavior rules the formation of oxidic phase, even after the partial isomorphic substitution of stable La(III) ions within the $Ce(OH)CO_3$ precursor. As a first step to assess the stability of binary samples obtained herein, TGA analysis was performed at 1 K min^{-1} heating rate, in order to have a closer insight of phase decomposition temperature. It was observed that heating rates of 5 K min^{-1} increased the observed transition temperature in almost 50 K.[24] Figure 4 presents the TGA trace of samples belonging to the Sm-Ce and Pr-Ce families; samples of the Gd-Ce family are presented in Figure S3. For all hexagonal $Ce_{1-x}Ln_x(OH)CO_3$ samples, the decomposition features are essentially similar to $Ce(OH)CO_3$ (sample Ce100), presenting only one main decomposition step of ca. 21% mass loss. For precursors holding increasing degrees of Ln(III) substitution the decomposition temperature, T_{desc}, continuously rises (see Figure 5) reaching the value reported for dehydroxilation the observed for bare $Ln(OH)CO_3$ (first step of decomposition, eq. 2). However, mass spectrometry coupled with TGA analysis revealed that CO_2 and H_2O are released simultaneously from Ce-Ln precursors, indicating that Ce(III) oxidation governs the process, according to eq. 1 (Figure S4). The slightly higher values of T_{desc} observed for Ce-Pr samples indicate that the eventual oxidation of Pr(III) is not driving the decomposition process. This shift can be interpreted in terms of a passive oxidic surface layer. For pure $Ln(OH)CO_3$ phases composed by non aliovalent lanthanides as Sm(III) or Gd(III), the formation of the oxide is preceded by a first step corresponding to a total dehydroxilation and a partial decarbonation processes to give a well-defined $Ln_2O_2CO_3$ crystalline phase (eq.2), that subsequently decompose to Ln_2O_3 at higher temperatures (eq.3).[28,42]

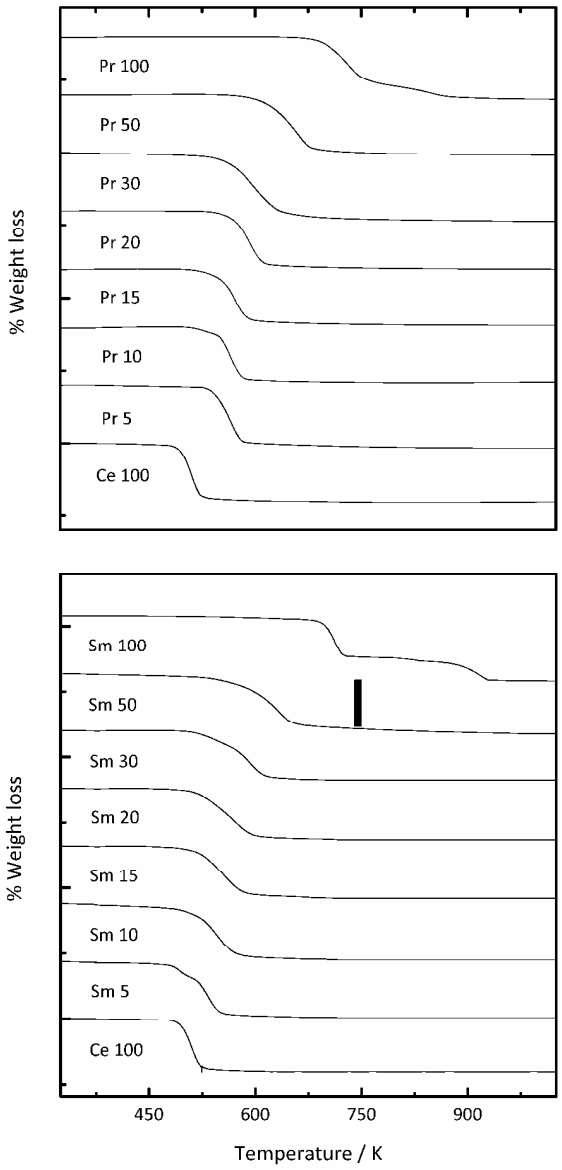

Figure 4 Thermogravimetric trace of $Ce_{1-x}Pr_x(OH)CO_3$ (upper panel) and $Ce_{1-x}Sm_x(OH)CO_3$ samples (lower panel) recorded at 1 K min^{-1} under air atmosphere. Scale bar represents a 21 % mass loss jump.

Pure carbonates evolve into their oxides in a single step (see eq. 4, Table 1). In the case of $Pr(OH)CO_3$ decomposition, dehydroxilation (eq. 5) precedes the partial oxidation of Pr(III) and the subsequent decarbonation (eq. 6), which leads to the well-defined mixed valence oxide, Pr_6O_{11} (PDF 42-1121), in which only two thirds of Pr ions reach the tetravalent state. However, further annealing completes the oxidation process (eq. 7), resulting in a PrO_2 phase isostructural with cerianite (CeO_2).[43–45]

Table 1. Thermal decomposition step of $Ce(OH)CO_3$, $Pr(OH)CO_3$, $Ln_2(CO_3)_3$ and $Ln(OH)CO_3$ being Ln a non aliovalent lanthanide.

Reaction in air atmosphere	T / K	Mass loss	Eq.
$^1/_4\ O_2 + Ce(OH)CO_3 \rightarrow CeO_2 + {}^1/_2\ H_2O + CO_2$	550 K	21 %	1
$2\ Ln(OH)CO_3 \rightarrow Ln_2O_2CO_3 + H_2O + CO_2$	700-800 K	14 %	2
$Ln_2O_2CO_3 \rightarrow Ln_2O_3 + CO_2$	980-1100 K	10 %	3
$Ln_2(CO_3)_3 \rightarrow Ln_2O_3 + 3\ CO_2$	700-800 K	27 %	4
$2\ Pr(OH)CO_3 \rightarrow Pr_2O_2CO_3 + H_2O + CO_2$	700 K	14.2 %	5
$O_2 + 3\ Pr_2O_2CO_3 \rightarrow Pr_6O_{11} + 3\ CO_2$	825 K	8.9 %	6
$^1/_2\ O_2 + Pr_6O_{11} \rightarrow 6\ PrO_2$	1100-1200 K	-2 %	7

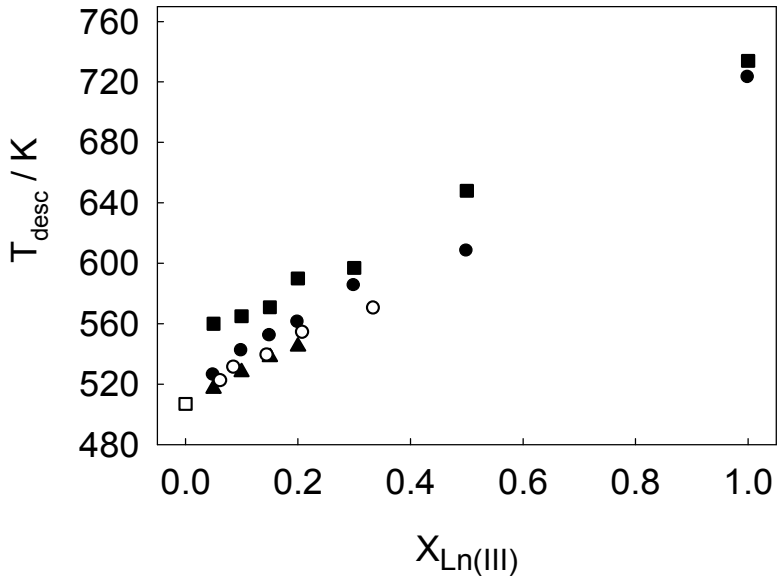

Figure 5. Temperature of decomposition, T_{desc}, of $Ce_{1-x}Ln_x(OH)CO_3$ precursors as a function of $X_{Ln(III)}$ for Ln(III)=Sm(III) (filled circles), Gd(III) (filled triangles) and Pr(III) (filled squares). Reference data from $Ce(OH)CO_3$ (empty square) and $Ce_{1-x}La_x(OH)CO_3$ (empty circles) from ref.[13] were also added.

3.4. Structure of Ln(III-IV)-Ce(IV) oxides

TGA analysis confirmed that massive decomposition of $Ce_{1-x}Ln_x(OH)CO_3$ can be achieved at moderate temperatures (723 K) for samples with $0<x<0.5$. The resulting oxides exhibit high specific surface areas of 70-130 m^2/g (see Table S1), indicating an average particle size of 7-8 nm.[24,41] PXRD inspection of $Ce_{1-x}Ln_x(OH)CO_3$ decomposed in air at 723 K (5 h) presents the main reflections of cubic CeO_2 except for the bare Ln(III) samples, that remains partially decomposed in the form of the correspondent oxocarbonate, $Ln_2O_2CO_3$, according to equations 2 and 5 (see Figures 6, 7 and ESI S5) .

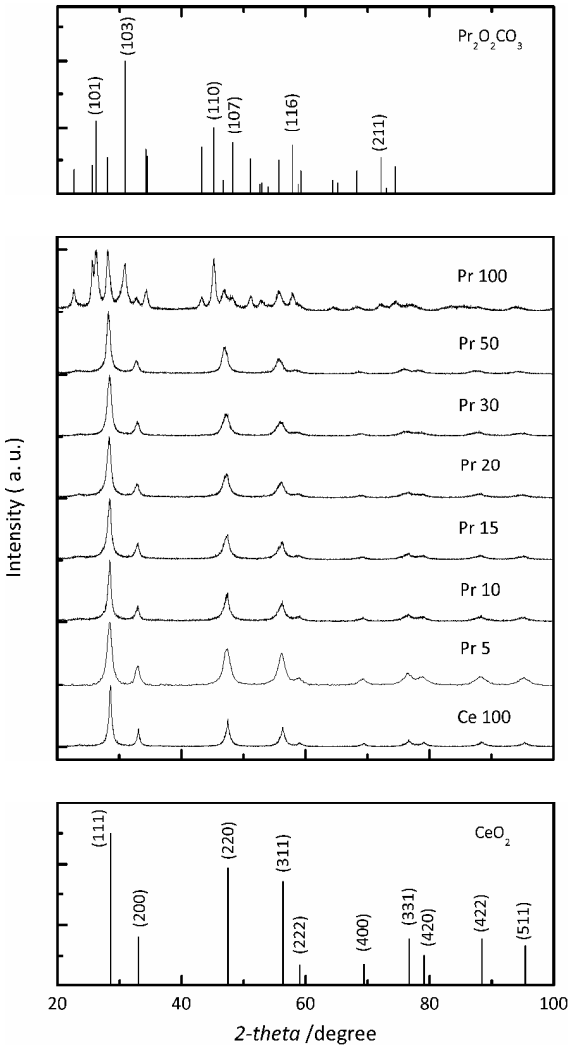

Figure 6. PXRD patterns of the oxides obtained after decomposition of $Ce_{1-x}Pr_x(OH)CO_3$ in air at 723 K. Upper panel: main reflections of $Pr_2O_2CO_3$ reference (PDF 37-0805). Lower panel: main reflections of cubic CeO_2 reference (PDF 65-2975).

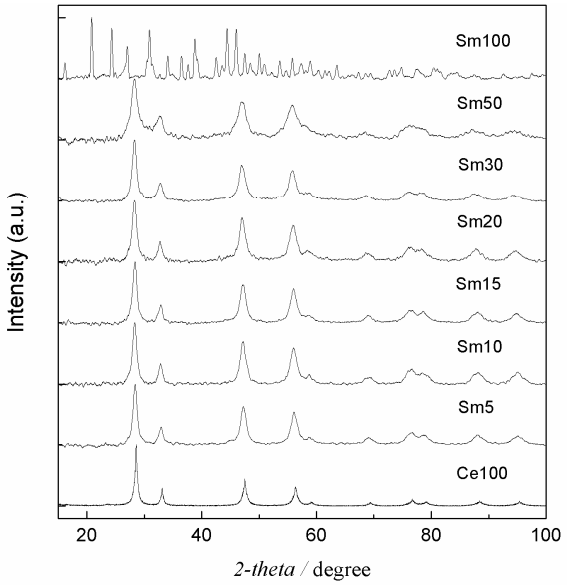

Figure 7. PXRD patterns of the oxides obtained after decomposition of $Ce_{1-x}Sm_x(OH)CO_3$ samples at 723 K (5 h, under air atmosphere).

Concerning the structural properties of the oxidic phases, the present samples were compared with related reference oxides reported elsewhere (see Figure 8). Both Gd(III) and Sm(III)-containing ceria phases revealed a cell expansion expectable for such cations. In both cases the values recorded of cell parameter exceed those predicted by well-established empirical models of Ln(III) substituted CeO_2.[46,47] This fact indicates the presence of a significant amount of Ce ions that remain in the trivalent state, as was observed for $Ce_{1-x}La_xO_{2-\delta}$ obtained under similar conditions.[48–53] Typically, the crystal coarsening and the massive oxidation of these Ce(III) defects start at 873 K.[54,55] In the case of, Ce(III)-Pr(III) family, the developed oxides depict a linear expansion of *a* parameter,[56,57] while these values remain in between those reported for Pr(III)-Ce(III-IV) and Pr(IV)-Ce(IV) oxide solid solutions, indicating the existence of a Pr(III-IV)-Ce(III-IV) oxide,[47,58] in good agreement with previous reports.[59]

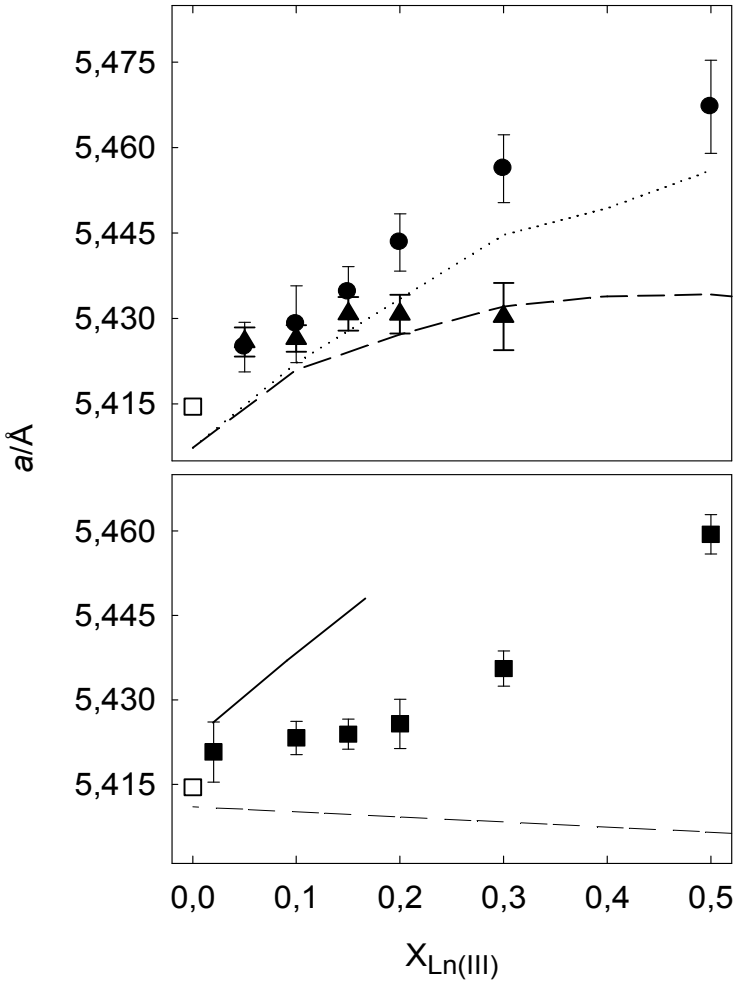

Figure 8. Upper panel: dependence of *a* cell parameter as a function of Ln(III) substitution, $X_{Ln(III),}$ for oxides obtained at 723 K containing Sm(III) (filled circles), Gd(III) (filled triangles). Dotted and dashed lines represents *a* values of Ce(IV)-Sm(III) and Ce(IV)-Gd(III) binary oxides, respectively (ref. 60). Lower panel: dependence of the *a* value vs. X_{Pr} for oxides obtained at 723 K (filled squares). Reference for Pr(III)-Ce(III-IV) (full line, ref. 58) and Pr(IV)-Ce(IV) (dashed line, ref. 46, 47) oxidic solid solutions are also included. In both panels, empty square represents bare Ce(IV-IIII) sample obtained at 723 K.

Electron microscopy based inspection of solids submitted to thermal decomposition revealed that the parent polycrystalline Ce(III)-Ln(III) basic carbonates develop subtle surface roughness, as was reported for related phases (see Fig. 9).[15] However, HRTEM inspection revealed that these particles consisted in stable mesoporous agglomerates of single crystalline oxide particles of a few nanometer

in diameter, in accordance with PXRD based estimations and surface area determinations (see Figure S6 and Table S1).[24,41]

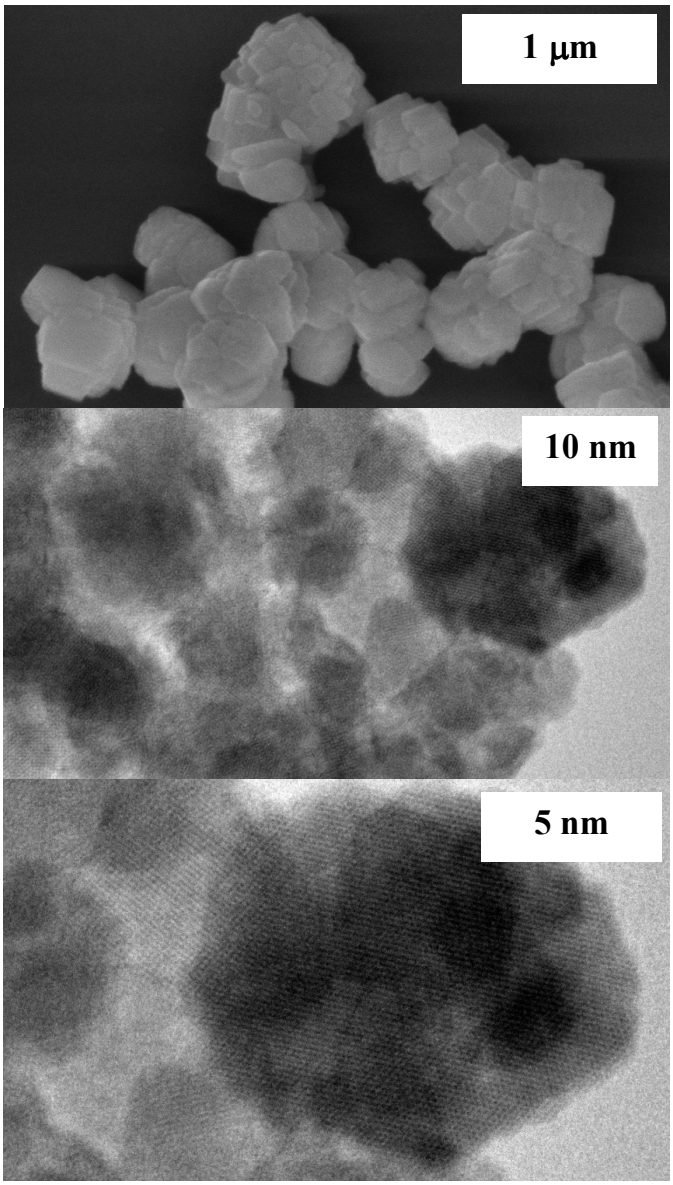

Figure 9. FESEM (upper panel) and HRTEM (middle and lower panel) images of sample Gd20 after thermal decomposition at 723 K.

4. Conclusions

Monophasic crystalline $Ce_{1-x}Ln_x(OH)CO_3$ hexagonal phases are effective precursors for the obtainment of pure nanocrystalline $Ce_{1-x}Ln_xO_{2-\delta}$ solid solutions in a single step of oxidative decomposition. Controlled low temperature decomposition preserves high surface area of the obtained oxidic solids, even higher than the values reported by advanced procedures. Because of the inherent tendency of Ln(III) to develop hexagonal basic carbonates, a variety of Ln(III)-Ce(III) phases, or even multicationic systems arise as very attractive precursors for the obtainment of complex ceria-based nanotextured multielement oxides.

Supporting information

PXRD, Coupled GA-MS determinations, N_2 sorption isotherms. This information is available free of charge via the Internet at http://pubs.acs.org.

Acknowledgements

This work was supported by Universidad de Buenos Aires (UBACyT 20020130100610BA), Agencia Nacional de Promoción Científica y Tecnológica (ANPCyT PICT 2012-1167) and Consejo Nacional de Investigaciones Científicas y Técnicas (CONICET PIP 11220110101020). CS and EAP acknowledge CONICET for doctoral fellowship. MJ is a Research Scientist of CONICET (Argentina). We deeply acknowledge Dr. Eugenio Otal for the TGA-MS measurements and Dr. Gervaise Mosser for the HRTEM images.

Bibliography

(1) Li, H.; Lu, G.; Wang, Y.; Guo, Y.; Guo, Y. Synthesis of Flower-like La or Pr-Doped Mesoporous Ceria Microspheres and Their Catalytic Activities for Methane Combustion. *Catal. Commun.* **2010**, *11* (11), 946–950.

(2) Montini, T.; Melchionna, M.; Monai, M.; Fornasiero, P. Fundamentals and Catalytic Applications of CeO_2-Based Materials. *Chem. Rev.*, **2016**, 116 (10), 5987–6041.

(3) Inaba, H.; Tagawa, H. Ceria-Based Solid Electrolytes. *Solid State Ionics* **1996**, No. 83, 1–16.

(4) Liu, W.; Flytzanistephanopoulos, M. Total Oxidation of Carbon Monoxide and Methane over Transition Metal Fluorite Oxide Composite Catalysts: I. Catalyst Composition and Activity. *J. Catal.* **1995**, *153* (2), 304–316.

(5) Avgouropoulos, G.; Ioannides, T.; Matralis, H.; Batista, J.; Hocevar, S. $CuO–CeO_2$ Mixed Oxide Catalysts for the Selective Oxidation of Carbon Monoxide in Excess Hydrogen. *Catal. Letters* **2001**, *73* (1), 33–40.

(6) Trovarelli, A.; de Leitenburg, C.; Boaro, M.; Dolcetti, G. The Utilization of Ceria in Industrial Catalysis. *Catal. Today* **1999**, *50* (2), 353–367.

(7) Funabiki, M.; Yamada, T.; Kayano, K. Auto Exhaust Catalysts. *Catal. Today* **1991**, *10* (1), 33–43.

(8) Muñoz, F. F.; Leyva, A. G.; Baker, R. T.; Fuentes, R. O. Effect of Preparation Method on the Properties of Nanostructured Gadolinia-Doped Ceria Materials for IT-SOFCs. *Int. J. Hydrogen Energy* **2012**, *37* (19), 14854–14863.

(9) Kharton, V. V; Figueiredo, F. M.; Navarro, L.; Naumovich, E. N.; Kovalevsky, A. V; Yaremchenko, A. A.; Viskup, A. P.; Carneiro, A.; Marques, F. M. B.; Frade, J. R. Ceria-Based Materials for Solid Oxide Fuel Cells. *J. Mater. Sci.* **2001**, *36* (5), 1105–1117.

(10) Fernández-García, M.; Martínez-Arias, A.; Hanson, J. C.; Rodriguez, J. A. Nanostructured Oxides in Chemistry: Characterization and Properties. *Chem. Rev.* **2004**, *104* (9), 4063–4104.

(11) Terribile, D.; Trovarelli, A.; Llorca, J.; de Leitenburg, C.; Dolcetti, G. The Synthesis and Characterization of Mesoporous High-Surface Area Ceria Prepared Using a Hybrid Organic/Inorganic Route. *J. Catal.* **1998**, *178* (1), 299–308.

(12) Crepaldi, E. L.; de A. A. Soler-Illia, G. J.; Bouchara, A.; Grosso, D.; Durand, D.; Sanchez, C. Controlled Formation of Highly Ordered Cubic and Hexagonal Mesoporous Nanocrystalline Yttria–Zirconia and Ceria–Zirconia Thin Films Exhibiting High Thermal Stability. *Angew. Chemie Int. Ed.* **2003**, *42* (3), 347–351.

(13) Soler-Illia, G. J. D. A. A.; Jobbágy, M.; Candal, R. J.; Regazzoni, A. E.; Blesa, M. A. Synthesis of Metal Oxide Particles from Aqueous Media: The Homogeneous Alkalinization Method. *J. Dispers. Sci. Technol.* **1998**, *19* (2–7), 207–228.

(14) Kandare, E.; Hossenlopp, J. M. Thermal Degradation of Acetate-Intercalated Hydroxy Double

and Layered Hydroxy Salts. *Inorg. Chem.* **2006**, *45* (9), 3766–3773.

(15) Go, Y. B.; Jacobson, A. J. Solid Solution Precursors to Gadolinia-Doped Ceria Prepared via a Low-Temperature Solution Route. *Chem. Mater.* **2007**, *19* (19), 4702–4709.

(16) Sorbello, C.; Barja, B. C.; Jobbágy, M. Monodispersed Ce(IV)–Gd(III)–Eu(III) Oxide Phosphors for Enhanced Red Emission under Visible Excitation. *J. Mater. Chem. C* **2014**, *2* (6), 1010–1017.

(17) Hu, L.; Ma, R.; Ozawa, T. C.; Sasaki, T. Synthesis of a Solid Solution Series of Layered $Eu_{(x)}Gd_{(1-x)}(OH)_{2.5}Cl_{0.5}\,0.9H_2O$ and Its Transformation into $(Eu_{(x)}Gd_{(1-x)})_2O_3$ with Enhanced Photoluminescence Properties. *Inorg. Chem.* **2010**, *49* (6), 2960–2968.

(18) Jobbágy, M.; Soler-Illia, G. J. D. A. A.; Regazzoni, A. E.; Blesa, M. A. Synthesis of Copper(II)-Containing Nickel(II) Hydroxide Particles as Precursors of Copper(II)-Substituted Nickel(II) Oxides. *Chem. Mater.* **1998**, *10* (6), 1632–1637.

(19) Klissurski, D.; Uzunova, E. Synthesis and Features of Binary Cobaltite Spinels. *J. Mater. Sci.* **1994**, *29* (2), 285–293.

(20) Rives, V. *Layered Double Hydroxides: Present and Future*; Rives, V., Ed.; Nova Science Publishers Inc.: New York, 2001.

(21) Li, F.; Liu, J.; Evans, D. G.; Duan, X. Stoichiometric Synthesis of Pure MFe_2O_4 (M = Mg, Co, and Ni) Spinel Ferrites from Tailored Layered Double Hydroxide (Hydrotalcite-Like) Precursors. *Chem. Mater.* **2004**, *16* (8), 1597–1602.

(22) Sileo, E. E.; Jobbágy, M.; Paiva-Santos, C. O.; Regazzoni, A. E. Thermal Decomposition of Crystalline NiII-CrIII Layered Double Hydroxide: A Structural Study of the Segregation Process. *J. Phys. Chem. B* **2005**, *109* (20), 10137–10141.

(23) Nguyen, T.-D.; Dinh, C.-T.; Do, T.-O. Two-Phase Synthesis of Colloidal Annular-Shaped $Ce_xLa_{1-x}CO_3OH$ Nanoarchitectures Assemblied from Small Particles and Their Thermal Conversion to Derived Mixed Oxides. *Inorg. Chem.* **2011**, *50* (4), 1309–1320.

(24) Jobbágy, M.; Sorbello, C.; Sileo, E. E. Crystalline Ce(III)-La(III) Double Basic Carbonates: A Chemical Shortcut to Obtain Nanometric La(III)-doped Ceria. *J. Phys. Chem. C* **2009**, *113* (25), 10853–10857.

(25) Rorif, F.; Fuger, J.; Desreux, J. F. Thermochemistry of Selected Trivalent Lanthanide and Americium Compounds: Orthorhombic and Hexagonal Hydroxycarbonates. *Radiochim. Acta/International J. Chem. Asp. Nucl. Sci. Technol.* **2005**, *93*, 103.

(26) Yang, H.; Dembowski, R. F.; Conrad, P. G.; Downs, R. T. Crystal Structure and Raman Spectrum of Hydroxyl-Bastnasite-(Ce), $CeCO_3(OH)$. *Am. Mineral.* **2008**, *93* (4), 698–701.

(27) Feng, W.-J.; Zhou, G.-P.; Liu, Z.-B.; Xu, Y. $Nd(CO_3)(OH)$ from Single-Crystal Data. *Acta Crystallogr. Sect. E* **2007**, *63* (9), i174.

(28) Park, I. Y.; Kim, D.; Lee, J.; Lee, S. H.; Kim, K.-J. Effects of Urea Concentration and Reaction Temperature on Morphology of Gadolinium Compounds Prepared by Homogeneous Precipitation. *Mater. Chem. Phys.* **2007**, *106* (1), 149–157.

(29) Lee, M.; Jung, W. Hydrothermal Synthesis of $LaCO_3OH$ and Ln^{3+}-Doped $LaCO_3OH$ Powders under Ambient Pressure and Their Transformation to $La_2O_2CO_3$ and La_2O_3. *Bull. Korean Chem. Soc.* **2013**, *34* (12), 3609–3614.

(30) Shannon, R. D. Revised Effective Ionic Radii and Systematic Studies of Interatomic Distances in Halides and Chalcogenides. *Acta Crystallogr. Sect. A* **1976**, *32* (5), 751–767.

(31) Kang, Z. C.; Eyring, L. Nanostructure Evolution during Chemical Processing of Gels: A High-Resolution Electron Microscope Study. 1. Rare Earth Oxide and Hydroxycarbonate Colloids. *J. Solid State Chem.* **1990**, *88* (1), 303–323.

(32) Sun, J.; Kyotani, T.; Tomita, A. Preparation and Characterization of Lanthanum Carbonate Hydroxide. *J. Solid State Chem.* **1986**, *65* (1), 94–99.

(33) Lechevallier, S.; Lecante, P.; Mauricot, R.; Dexpert, H.; Dexpert-Ghys, J.; Kong, H.-K.; Law, G.-L.; Wong, K.-L. Gadolinium−Europium Carbonate Particles: Controlled Precipitation for Luminescent Biolabeling. *Chem. Mater.* **2010**, *22* (22), 6153–6161.

(34) Candal, R. J.; Regazzoni, A. E.; Blesa, M. A. Precipitation of Monodispersed Mixed Copper-Gadolinium Basic Carbonate Particles. *Colloids Surfaces A Physicochem. Eng. Asp.* **1993**, *79* (2–3), 191–198.

(35) Aiken, B. A. R.; Hsu, W. A. N. P.; Matijevic, E. Preparation and Properties of Monodispersed Colloidal Particles of Lanthanide Compounds: III, Yttrium(III) and Mixed Yttrium(III)/Cerium(III) Systems. *J. Am. Ceram. Soc.* **1988**, *71* (10), 845–853.

(36) Li, J.-G.; Li, X.; Sun, X.; Ikegami, T.; Ishigaki, T. Uniform Colloidal Spheres for $(Y_{1-x}Gd_x)_2O_3$ (X = 0-1): Formation Mechanism, Compositional Impacts, and Physicochemical Properties of the Oxides. *Chem. Mater.* **2008**, *20* (6), 2274–2281.

(37) Li, J.-G.; Li, X.; Sun, X.; Ishigaki, T. Monodispersed Colloidal Spheres for Uniform Y_2O_3:Eu^{3+} Red-Phosphor Particles and Greatly Enhanced Luminescence by Simultaneous Gd^{3+} Doping. *J. Phys. Chem. C* **2008**, *112* (31), 11707–11716.

(38) Jobbágy, M.; Mariño, F.; Schönbrod, B.; Baronetti, G.; Laborde, M. Synthesis of Copper-Promoted CeO_2 Catalysts. *Chem. Mater.* **2006**, *18* (7), 1945–1950.

(39) Guo, Z.; Du, F.; Li, G.; Cui, Z. Synthesis and Characterization of Single-Crystal $Ce(OH)CO_3$ and CeO_2 Triangular Microplates. *Inorg. Chem.* **2006**, *45* (10), 4167–4169.

(40) Baranchikov, A. E.; Polezhaeva, O. S.; Ivanov, V. K.; Tretyakov, Y. D. Lattice Expansion and Oxygen Non-Stoichiometry of Nanocrystalline Ceria. *CrystEngComm* **2010**, *12* (11), 3531–3533.

(41) Poggio, E.; Jobbágy, M.; Moreno, M.; Laborde, M.; Mariño, F.; Baronetti, G. Influence of the Calcination Temperature on the Structure and Reducibility of Nanoceria Obtained from Crystalline $Ce(OH)CO_3$ Precursor. *Int. J. Hydrogen Energy* **2011**, *36* (24), 15899–15905.

(42) D'Assunção, L. M.; Ionashiro, M.; Rasera, D. E.; Giolito, I. Thermal Decomposition of the Hydrated Basic Carbonates of Lanthanides and Yttrium in CO_2 Atmosphere. *Thermochim. Acta* **1993**, *219*, 225–233.

(43) Sastry, R. L. N.; Yoganarasimhan, S. R.; Mehrotra, P. N.; Rao, C. N. R. Preparation, Characterization and Thermal Decomposition of Praseodymium, Terbium and Neodymium Carbonates. *J. Inorg. Nucl. Chem.* **1966**, *28* (5), 1165–1177.

(44) Sharma, R.; Hinode, H.; Eyring, L. A Study of the Decomposition of Praseodymium Hydroxy Carbonate and Praseodymium Carbonate Hydrate. *J. Solid State Chem.* **1991**, *92* (2), 401–419.

(45) Treu, B. L.; Fahrenholtz, W. G.; O'Keefe, M. J. Thermal Decomposition Behavior of Praseodymium Oxides, Hydroxides, and Carbonates. *Inorg. Mater.* **2011**, *47* (9), 974–978.

(46) Hong, S. J.; Virkar, A. V. Lattice Parameters and Densities of Rare-Earth Oxide Doped Ceria Electrolytes. *J. Am. Ceram. Soc.* **1995**, *78* (2), 433–439.

(47) Kim, D.-J. Lattice Parameters, Ionic Conductivities, and Solubility Limits in Fluorite-Structure MO_2 Oxide [M = Hf^{4+}, Zr^{4+}, Ce^{4+}, Th^{4+}, U^{4+}] Solid Solutions. *J. Am. Ceram. Soc.* **1989**, *72* (8), 1415–1421.

(48) Zhou, X.-D.; Huebner, W. Size-Induced Lattice Relaxation in CeO_2 Nanoparticles. *Appl. Phys. Lett.* **2001**, *79* (21), 3512.

(49) Zhang, F.; Jin, Q.; Chan, S.-W. Ceria Nanoparticles: Size, Size Distribution, and Shape. *J. Appl. Phys.* **2004**, *95* (8), 4319.

(50) Tsunekawa, S.; Fukuda, T.; Kasuya, A. Blue Shift in Ultraviolet Absorption Spectra of Monodisperse CeO_{2-X} Nanoparticles. *J. Appl. Phys.* **2000**, *87* (3), 1318–1321.

(51) Tsunekawa, S.; Sahara, R.; Kawazoe, Y.; Kasuya, A. Origin of the Blue Shift in Ultraviolet Absorption Spectra of Nanocrystalline CeO_{2-x} Particles. *Mater. Trans. JIM* **2000**, *41* (8), 1104–1107.

(52) Tsunekawa, S.; Sivamohan, R.; Ito, S.; Kasuya, A.; Fukuda, T. Structural Study on Monosize CeO_2 Nano-Particles. *Nanostructured Mater.* **1999**, *11* (1), 141–147.

(53) Patil, S.; Seal, S.; Guo, Y.; Schulte, A.; Norwood, J. Role of Trivalent La and Nd Dopants in Lattice Distortion and Oxygen Vacancy Generation in Cerium Oxide Nanoparticles. *Appl. Phys. Lett.* **2006**, *88* (24), 243110.

(54) Fernández-García, M.; Wang, X.; Belver, C.; Iglesias-Juez, A.; Hanson, J. C.; Rodriguez, J. A. Ca Doping of Nanosize Ce−Zr and Ce−Tb Solid Solutions: Structural and Electronic Effects. *Chem. Mater.* **2005**, *17* (16), 4181–4193.

(55) Kamruddin, M.; Ajikumar, P. K.; Nithya, R.; Tyagi, A. K.; Raj, B. Synthesis of Nanocrystalline Ceria by Thermal Decomposition and Soft-Chemistry Methods. *Scr. Mater.* **2004**, *50* (4), 417–422.

(56) Borchert, H.; Frolova, Y. V; Kaichev, V. V; Prosvirin, I. P.; Alikina, G. M.; Lukashevich, A. I.; Zaikovskii, V. I.; Moroz, E. M.; Trukhan, S. N.; Ivanov, V. P.; Paukshtis, E. A.; Bukhtiyarov, V. I.; Sadykov, V. A. Electronic and Chemical Properties of Nanostructured Cerium Dioxide Doped with Praseodymium. *J. Phys. Chem. B* **2005**, *109* (12), 5728–5738.

(57) Song, Z.; Liu, W.; Nishiguchi, H.; Takami, A.; Nagaoka, K.; Takita, Y. The Pr Promotion Effect on Oxygen Storage Capacity of Ce-Pr Oxides Studied Using a TAP Reactor. *Appl. Catal.*

A Gen. **2007**, *329*, 86–92.

(58) Rojas, T. C.; Ocaña, M. Uniform Nanoparticles of Pr(III)/Ceria Solid Solutions Prepared by Homogeneous Precipitation. *Scr. Mater.* **2002**, *46* (9), 655–660.

(59) Reddy, B. M.; Thrimurthulu, G.; Katta, L.; Yamada, Y.; Park, S.-E. Structural Characteristics and Catalytic Activity of Nanocrystalline Ceria−Praseodymia Solid Solutions. *J. Phys. Chem. C* **2009**, *113* (36), 15882–15890.

(60) Artini, C.; Pani, M.; Carnasciali, M. M.; Buscaglia, M. T.; Plaisier, J. R.; Costa, G. A. Structural Features of Sm- and Gd-Doped Ceria Studied by Synchrotron X-Ray Diffraction and μ-Raman Spectroscopy. *Inorg. Chem.* **2015**, *54* (8), 4126–4137.